BOND BEHVIOR OF FRP STRENGTHENING APPLIED ON CURVED MASONRY SUBSTRATES: NUMERICAL STUDY

Ernesto Grande[1*], Gabriele Milani[2], Antonio Formisano[3], Bahman Ghiassi[4], Francesco Fabbrocino[5]

[1]University Guglielmo Marconi, Department of Sustainability Engineering, Via Plinio 44, 00193 Roma, Italy. e.grande@unimarconi.it

[2]Politecnico di Milano, Department of Architecture, Built Environment and Construction Engineering (ABC), Piazza Leonardo da Vinci 32, 20133 Milano, Italy. gabriele.milani@polimi.it

[3]University of Naples Federico II, Department of Structures for Engineering and Architecture, PiazzaleTecchio 80, 80125 Napoli, Italy. antoform@unina.it

[4]University of Nottingham, Centre for Structural Engineering and Informatics, Faculty of Engineering, University of Nottingham, NG7 2RD, Nottingham, UK

[5]Pegaso Telematics University, Department of Engineering, Piazza Trieste e Trento 48, 80132 Napoli, Italy. francesco.fabbrocino@unipegaso.it

[*]corresponding author:
Ernesto Grande
[4]University Guglielmo Marconi
Department of Sustainability Engineering
via Plinio 44, 00193 Rome (Italy)
e.grande@unimarconi.it

ABSTRACT

The recent experimental and numerical studies concerning the local bond behavior of Fiber Reinforced Polymer (FRP) systems externally applied on curved masonry elements clearly underline the role of the geometric curvature on the performance of FRPs. In particular, the interaction between shear stresses and tension or compression normal stresses both arising at the FRP/masonry interface influences the bond strength and, consequently, the debonding behavior of FRPs. Then, the development of reliable numerical models able to predict the bond behavior of FRPs applied on curved masonry structures necessarily requires to consider this important feature which, on the contrary, is generally neglected in the case of flat substrates.

Aim of the present paper is to numerically investigate the bond behavior of FRP strengthening systems externally applied on curved masonry specimens. In particular, considering the simple spring-model approach proposed by the authors in previous research, a new constitutive law derived from the work of Thorenfeld et al. (1987) is here proposed by also considering the coupled behavior between shear and normal forces at the reinforcement/masonry interface. Numerical analyses are developed with reference to case studies deduced from the literature and consisting of shear-lap bond tests of curved masonry specimens characterized by different values of the geometric curvature and different strengthening configurations. The obtained results show the ability of the proposed modeling approach in capturing some effects, such as the beneficial friction effect when compression normal stresses develop at the interface level.

Keywords: FRP; debonding; masonry curved structures; spring-model.

INTRODUCTION

The current literature underlines the important role of the debonding phenomenon in the behavior of fiber reinforced strengthening systems externally applied to structural supports in the form of strips and sheets ([1]-[12]). Experimental investigations, mainly consisting in shear lap bond tests, are generally used for understanding the main features of this phenomenon, together with the role of different factors such as the type of the strengthening system, the characteristics of the masonry material composing the substrate, the modalities of application of the strengthening system, etc.([13]-[15]). The evidences emerged from these studies are generally considered for the development and validation of numerical and theoretical models aimed at reproducing the debonding phenomenon of both fiber reinforced polymers (FRP) and fiber reinforced cementitious grout (FRCM) applied to structural substrates ([16]-[24]). In particular, according to the experimental evidences, the majority of theoretical and numerical models available in the current literature are based on the main assumption that, during the debonding process, the damage only affects a thin layer of the material placed between the FRP-strengthening and the substrate (denoted interface), whilst the other components (substrate and FRP-strengthening) behave in the elastic stage. Moreover, the most common interface modeling approaches available in literature are based on the introduction of cohesive zones at the interface level by assuming a debonding mechanism which occurs under the tangential loading only or largely dominated by this failure mode (mode II). This last assumption, which results realistic for FRPs applied on substrates with a flat configuration, where the shear behavior is the predominant mechanism, could be not adequate in case of applications on curved substrates, where, on the contrary, the coupling between the mode II and the mode I mechanisms assumes a relevant role in the debonding process ([25]-[27]).

In this context, Grande and Milani ([28]) have recently proposed a simple but effective numerical model for the study of the bond behavior of FRPs externally applied on curved masonry substrates which straightforwardly introduces at the interface level coupled cohesive laws for considering a mixed mode de-bonding mechanism. A similar approach was also presented in [29], where taking

into account the important role of the coupling between shear and normal forces developing at the FRP/substrate interface level, the authors also introduced specific constitutive laws able to account for the friction effect in the de-bonding phase when compression forces arise at the reinforcement/substrate interface. The ability of the proposed approach was assessed by the authors by both considering the experimental tests reported in [27] and the numerical analyses developed in [30] obtained by using advanced F.E. models.

In this paper it is presented a numerical study concerning the debonding phenomenon of curved masonry specimens strengthened by FRPs. In particular, considering the spring-model presented in [28], the authors propose the use of constitutive laws for both the tangential and the normal behavior of the FRP/substrate interface derived on the basis of the law proposed in [31]. The main difference with respect to the other similar models of literature is the use of a unique constitutive law for the shear behavior of the interface which allows to capture the beneficial effect of friction on the bond strength when compression forces develop at the FRP/masonry interface. In other words, differently for the model presented in [29], the approach here presented does not require to introduce specific conditions for the constitutive law of the interface in presence of normal stresses.

The numerical analyses presented in the paper with reference to case studies derived from the current literature show the reliability of the proposed modeling approach. In particular, it is underlined the ability of the proposed laws to capture the effect of friction due to normal stresses in compression arising at the interface level, without introducing additional conditions in the coupling behavior.

SPRING-MODEL APPROACH

Recently, some of the authors of this paper have presented a simple 1D-spring model for the study of the debonding behavior of curved masonry specimens strengthened by FRPs ([28], [29]). The model consists in a simple schematization by using linear and nonlinear spring elements (Figure 1). In particular, springs with a linear-elastic behavior are specifically introduced to model the masonry substrate and the FRP-strengthening, which are then assumed behave linear-elastically, whilst two

types of zero-length nonlinear springs are introduced for the interface layer. Indeed, springs which only activate for the tangential component of the relative displacement between the strengthening and the substrate nodes (denoted in the following as 'interface shear spring') are introduced to account for the mode II mechanism; springs which only activate for the component of the relative displacement between the strengthening and the substrate nodes orthogonal to the substrate (denoted in the following as 'interface normal spring'), are introduce to account for the mode I mechanism.

On the basis of this schematization, the element stiffness matrix and then the corresponding global one, results dependent on both the tangential and normal relative displacements between the strengthening and the substrate. This represents one of the main features of the proposed modeling approach since it allows to account for the coupling between the tangential and normal behavior of the interface during the debonding process.

CONSTITUTIVE LAWS AND COUPLED BEHAVIOR

Different from the schematization proposed in ([28], [29]), where simple bilinear laws together with specific conditions based on the sign of normal stresses developing at the interface level (compression or tension) were introduced for the schematization of the behavior of the interface springs, the approach here proposed is based on the use of a unique constitutive law derived from the one proposed in [31]. The introduction of this law allows to directly accounts for the effect of normal stresses at the interface level on the tangential behavior without introducing additional conditions in the post peak stage ([29]).

Then, considering the force-displacement T-Δ law proposed in [31]:

$$T(\Delta) = T_b \frac{\Delta}{\Delta_0} \left[\frac{n}{n-1+\left(\frac{\Delta}{\Delta_0}\right)^{nk}} \right] \qquad \text{eqn. 1}$$

where T_b is the peak force, Δ_0 is the displacement corresponding to the peak force, n and k are two coefficients, the role of these coefficients on the shape of the law is preliminary investigated. In

particular, it can be observed that, while the coefficient k influences the peak force T_b, the corresponding displacement Δ_0 and the slope of the pre and post-peak branch (see Figure 2), the coefficient n does not affect neither the peak force T_b nor the corresponding displacement Δ_0, but only the slope of the pre and post-peak branch of the curve (see Figure 3).

On the basis of these evidences, the law proposed in [31] is here assumed for both tangential and normal springs composing the spring-model, respectively in terms of T_t-Δ_t and T_n-Δ_n laws, by assuming a unitary value for the coefficient k and a value of the coefficient n calibrated on the fracture energy G^I, G^{II} related to the mode I and the mode II respectively:

$$T_t(\Delta_t) = T_{t,b}\frac{\Delta_t}{\Delta_{t,0}}\left[\frac{n_t}{n_t - 1 + \left(\frac{\Delta_t}{\Delta_{t,0}}\right)^{n_t}}\right] \quad \text{eqn. 2}$$

$$T_n(\Delta_n) = T_{n,b}\frac{\Delta_n}{\Delta_{n,0}}\left[\frac{n_n}{n_n - 1 + \left(\frac{\Delta_n}{\Delta_{n,0}}\right)^{n_n}}\right] \quad \text{eqn. 3}$$

where: $T_{t,b}$ and $T_{n,b}$ are the peak forces of the constitutive laws of shear and normal springs respectively; $\Delta_{t,0}$ and $\Delta_{n,0}$ are the displacements corresponding to the peak force of shear and normal springs respectively; n_t and n_c are the coefficients evaluated on the facture energy of mode I and mode II respectively.

In addition to the accounted constitutive laws, the influence of the forces T_n arising in the interface normal springs (forces in compression or tension) on the forces T_t of the corresponding interface shear springs, is specifically introduced in the model by considering the Mohr-Coulomb failure domain:

$$T_t = T_{t,b} - T_n \tan(\psi) \quad \text{eqn. 4}$$

where ψ is the friction angle characterizing the yield domain.

Then, considering the accounted spring laws and the structure of the algorithm at the basis of the spring-model, the secant stiffness K_{sec} including the effect of T_t-T_n coupling behavior is derived:

$$K_{\sec}(\Delta_t, \Delta_n, \tan(\Psi)) = K_t \cdot \alpha(\Delta_t, \Delta_n, \tan(\Psi)) \quad \text{eqn. 5}$$

where K_t is the secant stiffness corresponding to the attainment of $T_{t,b}$:

$$K_t = \frac{T_{t,b}}{\Delta_{t,0}} \quad \text{eqn. 6}$$

and α is a coefficient which accounts for both the shape of the T_t-Δ_t law and the T_t-T_n coupling effect:

$$\alpha = \alpha_t - \alpha_n \frac{K_n}{K_t} \frac{\Delta_n}{\Delta_t} \tan(\Psi) \quad \text{eqn. 7}$$

where:

$$\alpha_t = \frac{n_t}{n_t - 1 + \left(\frac{\Delta_t}{\Delta_{t,0}} \right)^{n_t}} \quad \text{eqn. 8}$$

$$\alpha_n = \frac{n_n}{n_n - 1 + \left(\frac{\Delta_n}{\Delta_{n,0}} \right)^{n_n}} \quad \text{eqn. 9}$$

$$K_n = \frac{T_{n,b}}{\Delta_{n,0}} \quad \text{eqn. 10}$$

The coefficient α is introduced in the element stiffness matrix without modifying the structure of the problem proposed in [28] and implemented in Matlab[32] throughout an iterative procedure based on the classic Newton-Raphson technique by selecting the displacement control approach.

NUMERICAL APPLICATIONS

Numerical applications are carried out by using the spring-model proposed in [28] together with the constitutive laws and the coupled model here proposed. In particular, case studies derived from the literature and consisting of curved masonry specimens strengthened by FRPs are considered.

CASE STUDIES

Although numerous practical applications of FRP strengthening systems involve curved masonry structures (arches, vaults, domes, etc.), only few studies concerning the local bond behavior of FRP

applied on curved substrates are now available in the current literature. In the present paper, two sets of case studies are considered.

The first set of specimens (see Figure 4.a-d) refers to the experimental study carried out in [27], where single shear-lap bond tests of masonry pillars externally strengthened by FRP strips and characterized by different curvature radius and strengthening configurations were developed. In particular, as shown in Figure 4, four types of specimen in terms of curvature radius and strengthening configuration compose the accounted set:

- curved masonry specimen characterized by a radius equal to 1500 mm (denoted R150) strengthened at the intrados;
- curved masonry specimen characterized by a radius equal to 1500 mm (denoted R150) strengthened at the extrados;
- curved masonry specimen characterized by a radius equal to 3000 mm (denoted R300) strengthened at the intrados;
- curved masonry specimen characterized by a radius equal to 3000 mm (denoted R300) strengthened at the extrados.

All the masonry specimens were assembled by using five clay bricks with interposed mortar joints made of lime and cement as binder which main properties were experimentally derived in [27] and here summarized in Table 1. On the other hand, the reinforcement characterizing the specimens was made of a 100 mm wide unidirectional carbon fiber textile glued on the masonry prisms by means of a thin layer of epoxy resin (see Table 1).

The single lap shear tests were performed in [27] by pulling the top edge of the carbon fabric left unbounded. The specimens were constrained by a steel plate at the upper base and by a steel wedge at the lower base. Both the upper plate and the lower wedge were linked by four steel bars to ensure the stability of the specimens during the tests. In addition, the steel wedge was equipped with an additional steel plate to constrain the specimen toward its rotation. Further details can be found in [27].

In addition to shear lap tests, pull-off tests on reinforced bricks in compliance with [33] were also performed in [27] in order to evaluate the bond strength between the CFRP reinforcement and the substrate evaluated by simply dividing the maximum pull-off force by the cross section area of the partial core: an average value equal to 1.15 MPa was obtained in [27].

The second set of specimens here accounted for the numerical analyses are the curved masonry specimens reinforced with GFRP (Figure 4.e,f) employed for an experimental investigation carried out at the University of Minho (Portugal), where single shear lap bond tests were performed with the main purpose to experimentally investigate the role of the geometry curvature on the debonding mechanism [26]. In this case, the specimens were made by using four Portuguese Galveias clay bricks jointed by three thick mortar joints constituted by conventional mortar commercially available. Specimens characterized by flat external surfaces, exception made for the strengthened surface, which has a constant curvature of radius R_0=760 mm were obtained (Figure 4). The obtained overall size of the samples was about 235x130x90 mm^3 with a strengthening system characterized by GFRP strips with a bond length equal to 150 mm. Moreover, during the tests, two geometries with the same radius of the curvature were considered: one convex and the other concave. The tests were conducted through an ad-hoc delamination test setup with experimental tests conducted under displacement control (0.1 mm/min prescribed 7stroke speed). In addition, the specimens were instrumented with LVDTs applied directly on the fiber. During the tests, the imposed incremental displacement was applied at the free end of the strip considering an unbonded length equal to 110 mm. The main characteristics of masonry and strengthening materials are summarized in Table 1.

PARAMETERS SETTING

Regarding the parameters characterizing the numerical models, they are summarized in Table 2. In particular, the following parameters setting procedure has been considered in the present paper:

- the peak forces $T_{t,b}$ and $T_{n,b}$ of the shear and normal springs have been obtained by directly considering the values of the bond strength τ_0 and tensile strength f_t used in [28] and [30]: they have

been multiplied by the corresponding cross section area of the shear and normal spring for obtaining $T_{t,b}$ and $T_{n,b}$ respectively;

- the displacements at the peak $\Delta_{t,0}$ and $\Delta_{n,0}$ of the T_t-Δ_t and T_n-Δ_n laws have been assumed equal to the corresponding displacements $\Delta_{t,0}$ and $\Delta_{n,0}$ of the bi-linear laws used in [28] and [30];

- an ultimate value of the displacement of shear springs $\Delta_{t,f}$ equal to the displacement corresponding to the end of the descending branch characterizing the bi-linear laws used in [28] and [30], has been considered in order to identifying the beginning of the detachment phenomenon of the reinforcement;

- the parameters n_t and n_c have been obtained by considering the fracture energy values characterizing the bi-linear laws used in [28] and [30].

The comparison between the bi-linear law and the corresponding Thorenfeldt's law for the shear behavior of the interface is presented in Figure 5 for the two accounted series of specimens. From the plots it is important to observe that, differently from bilinear laws (dotted lines), where a null residual strength is commonly assumed due to a sudden release of energy, the proposed laws are characterized by a residual post-peak strength. This feature of the proposed law is strictly related to the parameters setting procedure where the same fracture energy is imposed in order to guarantee the same level of energy dissipation. Moreover, although the residual bond strength, which in the case of flat substrates is mainly due to the interlocking phenomenon inside the masonry composing the interface, is generally neglected, it can have a relevant role in case of curved substrates because of the activation of the friction due to the presence of compression normal stresses.

RESULTS

The results obtained from the numerical analyses are reported in Figure 6 in terms of force-displacement curves. In each plot of the figure are compared the curves obtained from the experimental tests (thin black lines) and those deduced from the numerical analyses (thick red lines). Form the figure it is possible to observe that the numerical force-displacement curves of both the sets of the accounted specimens show a good fitting performance of the global response of specimens.

Indeed, it is evident the ability of the proposed model to capture the influence of both the curvature of the masonry substrate (first set of specimens) and the configuration of the strengthening (first and second set of specimens) on the bond behavior of specimens. Indeed, as expected, greater values of the peak load emerge in the case of strengthening applied at the extrados respect to the application at the intrados, and this effect is influenced by the radius of curvature.

Moreover, in the case of the first set of specimens it is particular evident that the post-peak behavior of specimens strengthened at the extrados is characterized by a more remarkable hardening effect respect to the ones strengthened at the intrados (effect emerged from experimental tests and also from the numerical analyses). As observed in [28] and [29], this effect is mainly due to the value of the residual bond strength which depends on the friction phenomenon activated by compression normal stresses developing at the FRP/substrate interface. Indeed, in [29] the authors specifically introduced a three-linear law where the last horizontal branch simulates this effect. In this paper, the use of the Thorenfeldt's law, together with the Mohr-Coulomb coupled model, automatically allows to account for this effect without introducing in the model additional instructions about the evolution of the post-peak branch of shear stress-slip constitutive law.

Nevertheless, although the above considerations have a general validity, it is important to observe that the global bond behavior of specimens is particularly influenced by both their configuration and, also, by the characteristics of the substrate and strengthening materials. Indeed, the second set of specimens (i.e. the ones accounted in [26]), characterized by a greater radius with respect to the first set, but by a lower bond length of strips, showed a global response characterized by a suddenly strength decrease in both convex and concave specimens (behavior also underlined by the numerical analyses).

Indeed, using the proposed model, it is possible to observe that in the case of the convex specimen of the second set (Figure 4.e), the attainment of the peak load corresponds to a condition where the majority of the interface shear springs are in the post-peak stage with a tangential displacement

$\Delta_{t,0} < \Delta_t < \Delta_{t,f}$ (Figure 7). This is mainly due to the reduced value of the bond length which leads to a rapid degradation of the bond force.

Finally, the comparison between the experimental and numerical curves shows displacement values corresponding to the attainment of the peak load of the numerical curves lower than the one corresponding to the experimental curves. This outcome is probably due to the simplifications of the proposed model which does not consider the presence of mortar joints, their possible damage and, in particular, does not account for three-dimensional effects which generally contribute to mitigate stress concentrations at the FRP/substrate interface [34].

CONCLUSIONS

Although several applications of FRPs just involve curved structures (arches, vaults, domes, etc.), the debonding phenomenon of FRPs applied on curved masonry substrates is a topic still scarcely investigated. The few experimental and theoretical studies available in the recent literature underline differences with respect to the debonding occurring in case of FRPs applied on flat substrates and, at the same time, the common theoretical/numerical models are in some case not adequate because of assumptions only valid in the case of flat substrates.

The study presented in this paper is in the continuation of a research activity aimed at developing simple models based on the interface concept for the study of the debonding phenomenon of curved masonry specimens strengthened with FRPs. Here, in particular, the attention is focused on the use of constitutive laws opportunely derived from studies available in literature, able to capture specific features, such as the beneficial friction effect due to compression normal stresses arising at the interface level.

The numerical analyses presented in the paper have been developed by combining the proposed laws with the spring-model proposed in [28] and considering some case studies selected from literature. Before presenting the obtained results, it has been outlined the phase of parameters setting. In particular, it has been underlined that the parameters characterizing the proposed law correspond to

the outcomes generally obtained from common shear lap tests of specimens with flat surfaces used for deriving the peak shear force $T_{t,b}$ and the fracture energy of the mode II, and pullout tests for evaluating the normal strength used for deriving the the peak normal force $T_{n,b}$ and the fracture energy of the mode I. This allows a practical use of the proposed law.

The obtained results, mainly presented in terms of global response of specimens, have emphasized the ability of the proposed approach to predict the debonding phenomenon of curved masonry specimens strengthened by FRPs. In particular, the model is able to capture effects strictly related to the geometry of specimens (curvature radius) and also to the strengthening configuration (FRP applied at the intrados or extrados). In particular, the effect of normal stresses arising at the interface level is well captured in the post-peak stage of the global response.

These results are in agreement with the ones reported in [29]: they indeed underline the role of the coupling behavior between shear and normal stresses, and the effect of compressive stresses developing at the FRP/masonry interface in increasing the bond strength and the global bond resistance of specimens. On the other hand, differently from [29], where an horizontal post-peak branch of the force-displacement curves is observed in the specimens when normal stresses in tension arise at the FRP/masonry interface (this outcome is strictly related to the assumption of a null value of the residual shear strength), the accounted residual strength of the law proposed in this paper, which of course decreases in the presence of normal forces in tension, leads to a global response characterized by a sloping post-peak branch with a lower slope with respect to the case of normal stresses in compression.

REFERENCES

[1] Aiello MA, Sciolti MS, Triantafillou TC. FRP- strengthened masonry: Bond aspects. FRPRCS-8 (CD-ROM) Univ of Patras. Patras, Greece 2007.

[2] Oliveira D, Basilio I, Lourenço PB. Experimental bond behavior of FRP sheetsglued on brickmasonry. ASCE J. ComposCons 2011;15(1):32–41.

[3] Grande E, Imbimbo M, Sacco E. Bond behavior of CFRP laminatesglued on claybricks: experimental and numericalstudy. Compos Part B Eng 2011;42(2):330–40.

[4] Grande E, Imbimbo M, Sacco E. Bond Behavior of Historical Clay BricksStrengthened with Steel ReinforcedPolymers (SRP). Materials. 2011;4(3):585-600.

[5] Ghiassi B, Xavier J, Oliveira D V., Lourenço PB. Application of digital image correlation in investigating the bond between FRP and masonry. ComposStruct 2013. doi:10.1016/j.compstruct.2013.06.024.

[6] Ghiassi B, Marcari G, Oliveira D V., Lourenço PB. Numericalanalysis of bond behaviorbetweenmasonrybricks and composite materials. EngStruct 2012. doi:10.1016/j.engstruct.2012.05.022.

[7] Ghiassi B, Oliveira D V., Lourenço PB, Marcari G. Numericalstudy of the role of mortarjoints in the bond behavior of FRP-strengthened masonry. Compos Part B Eng 2013. doi:10.1016/j.compositesb.2012.10.017.

[8] Ghiassi B, Verstrynge E, Lourenço PB, Oliveira D V. Characterization of debonding in FRP-strengthenedmasonryusing the acousticemissiontechnique. EngStruct 2014. doi:10.1016/j.engstruct.2014.01.050.

[9] Maljaee H, Ghiassi B, Lourenço PB, Oliveira D V. FRP-brickmasonry bond degradation under hygrothermalconditions. ComposStruct 2016. doi:10.1016/j.compstruct.2016.03.037.

[10] Ghiassi B, Xavier J, Oliveira D V., Kwiecien A, Lourenço PB, Zajac B. Evaluation of the bond performance in FRP-brickcomponents re-bondedafterinitial delamination. ComposStruct 2015. doi:10.1016/j.compstruct.2014.12.047.

[11] de Felice G, De Santis S, Garmendia L, Ghiassi B, Larrinaga P, Lourenço PB, et al. Mortar-basedsystems for externallybondedstrengthening of masonry. Mater StructConstr 2014. doi:10.1617/s11527-014-0360-1.

[12] Ghiassi B, Razavizadeh A, Oliveira D V., Marques V, Lourenço PB. Tensile and bond characterization of natural fibers embeeded in inorganic matrices. RILEM Bookseries, 2016. doi:10.1007/978-94-017-7515-1_23.

[13] Valluzzi MR, Oliveira DV, Caratelli A, Castori G, Corradi M, de Felice G, et al. Round Robin Test For Composite-To-Brick Shear Bond Characterization. Mat and Struct - RILEM. 2012; 45(12):1761–1791.

[14] Grande E, Imbimbo M, Sacco E. Investigation on the bond behavior of clay bricks reinforced with SRP and SRG strengthening systems. Materials and Structures 2015; 48(11): 3755-70.

[15] Capozucca R, Ricci V. Bond of GFRP strips on modern and historic brickwork masonry. Composite Structures, 2016, 140: 540–555.

[16] Grande E, Imbimbo M, Sacco E. Bond behavior of CFRP laminates glued on clay bricks: experimental and numerical study. Compos Part B Eng 2011;42(2):330–40.

[17] Grande E, Imbimbo M. The role of the adhesive on the bond behavior of SRPs applied on masonry supports: Experimental and numerical study. Key Engineering Materials. 2015;624:652-659.

[18] Grande E, Imbimbo M, Sacco E. Simple model for the bond behavior of masonry elements strengthened with FRP. J Compos Constr 2011;15 (3):354–63.

[19] Grande E, Milani G, Sacco E. Modelling and analysis of FRP-strengthened masonry panels. Engineering Structures. 2008;30(7): 1842-1860.

[20] Grande E, Imbimbo M, Sacco E. A beam finite element for the nonlinear analysis of masonry buildings strengthened with FRP. International Journal of Architectural Heritage. Conservation, Analysis, and Restoration. 2011;5(6):693-716.

[21] Grande E, Imbimbo M. A simple 1D-Finite Element approach for the study of the bond behavior of masonry elements strengthened by FRP. Composites Part B. 2016;91:548-558.

[22] Grande E, Imbimbo M, Sacco E. Numerical investigation on the bond behavior of FRCM strengthening systems. Compos Part B Eng 2018;145. doi:10.1016/j.compositesb.2018.03.010.

[23] Grande E, Imbimbo M, Sacco E. Local bond behavior of FRCM strengthening systems: Some considerations about modeling and response. vol. 747 KEM. 2017. doi:10.4028/www.scientific.net/KEM.747.101.

[24] Grande E, Milani G. Interface modeling approach for the study of the bond behavior of FRCM strengthening systems. Compos Part B Eng 2018;141. doi:10.1016/j.compositesb.2017.12.052

[25] Malena M, de Felice G. Externally bonded composites on a curved masonry substrate: experimental results and analytical formulation. Composite Structures 2014; 112(1): 194-206.

[26] Basilio I. Strengthening of arched masonry structures with composite materials. PhD thesis, University of Minho, Department of Civil Engineering, Portugal October 2007.

[27] Rotunno T, Fagone M, Bertolesi E, Grande E, Milani G. Single lap shear tests of masonry curved pillars externally strengthened by CFRP strips. Compos Struct. 2018. http://dx.doi.org/10.1016/j.compstruct.2018.05.097.

[28] Grande E, Milani G. Modeling of FRP-strengthened curved masonry specimens and proposal of a simple design formula. Compos Struct 2016;158:281–90.

[29] Grande E, Fagone M, Rotunno T, Bertolesi E, Milani G. Coupled interface-based modelling approach for the numerical analysis of curved masonry specimens strengthened by CFRP. Composite Structures 200 (2018) 498–506.

[30] Bertolesi E, Milani G, Fagone M, Rotunno T, Grande E. Micro-mechanical FE numerical model for masonry curved pillars reinforced with FRP strips subjected to single lap shear tests. Composite Structures 201 (2018) 916–931.

[31] Thorenfeldt, E., Tomaszewicz, A., and Jensen, J. J. Mechanical properties of high-strength concrete and applications in design. In Proc. Symp. Utilization of High-Strength Concrete (Stavanger, Norway) (Trondheim, 1987), Tapir.

[32] MATLAB version 7.10.0. Natick, Massachusetts: The MathWorks Inc.; 2010.

[33] ASTM C1583/C1583M-13. Standard Test Method for Tensile Strength of Concrete Surfaces and the Bond Strength or Tensile Strength of Concrete Repair and Overlay Materials by Direct Tension (Pull-off Method) 2013.

[34] Fedele R, Milani G. Three-dimensional effects induced by FRP-from-masonry delamination. Compos Struct 2011;93(7):1819–31.

Table 1. Characteristics of materials composing the specimens accounted for the numerical analyses.

(Rotunno et al., 2018)			
bricks	average compressive strength	f_{bc} [MPa]	20.1
	average tensile strength	f_{bt}[MPa]	2.5
	average Young's modulus	E_b [MPa]	8712
mortar	average compressive strength	f_{mc} [MPa]	20.1
	average tensile strength (bending)	f_{mt} [MPa]	2.5
strengthening	nominal thickness	t_f [mm]	0.165
	tensile elastic modulus	E_f[MPa]	250000
	ultimate tensile strain	ε_f [%]	1.3
	characteristic tensile strength	f_{ft} [MPa]	3200
(Basilio, 2017)			
bricks	average compressive strength	f_{bc} [MPa]	8.2
	average Young's modulus	E_b [MPa]	3280
mortar	average compressive strength	f_{mc} [MPa]	7.3
	average tensile strength (bending)	f_{mt} [MPa]	1800
strengthening	nominal thickness	t_f[mm]	0.149
	tensile elastic modulus	E_f[MPa]	65000
	ultimate tensile strain	ε_f [%]	4.3
	characteristic tensile strength	f_{ft}[MPa]	3000

Table 2. Parameters characterizing the interface springs.

parameters used for the specimens of Rotunno et al. (2018) – [ref. Bertolesi et al., 2018]			
interface shear behavior	bond shear strength	τ_0 *[MPa]*	1.1915
	fracture energy	Γ_{ft} *[N/mm]*	0.2383
	coefficient of the Thorenfeldt's law	n_t	1.4
	slip at the end of the ascending branch	$\Delta_{t,0}$ *[mm]*	0.011
	slip at the end of the descending branch	$\Delta_{t,f}$ *[mm]*	0.4
interfacenormalbehaviour	tensile strength	f_t *[N/mm^2]*	1.15
	coefficient of the Thorenfeldt's law	n_c	2.4
	slip at the end of the ascending branch	$\Delta_{n,0}$ *[mm]*	0.0015
	slip at the end of the ascending branch	$\Delta_{n,f}$ *[mm]*	0.015
parameters used for the specimens of Basilio (2017) – [ref. Grande and Milani, 2016]			
interfaceshearbehavior	bond shear strength	τ_0 *[MPa]*	1.23
	fracture energy	Γ_{ft} *[N/mm]*	1.52
	coefficient of the Thorenfeldt's law	n_t	1.28
	slip at the end of the ascending branch	$\Delta_{t,0}$ *[mm]*	0.030
	slip at the end of the descending branch	$\Delta_{t,f}$ *[mm]*	2.48
interfacenormalbehaviour	tensile strength	f_t *[N/mm^2]*	0.87
	coefficient of the Thorenfeldt's law	n_c	2.4
	slip at the end of the ascending branch	$\Delta_{n,0}$ *[mm]*	0.0078
	slip at the end of the ascending branch	$\Delta_{n,f}$ *[mm]*	0.042

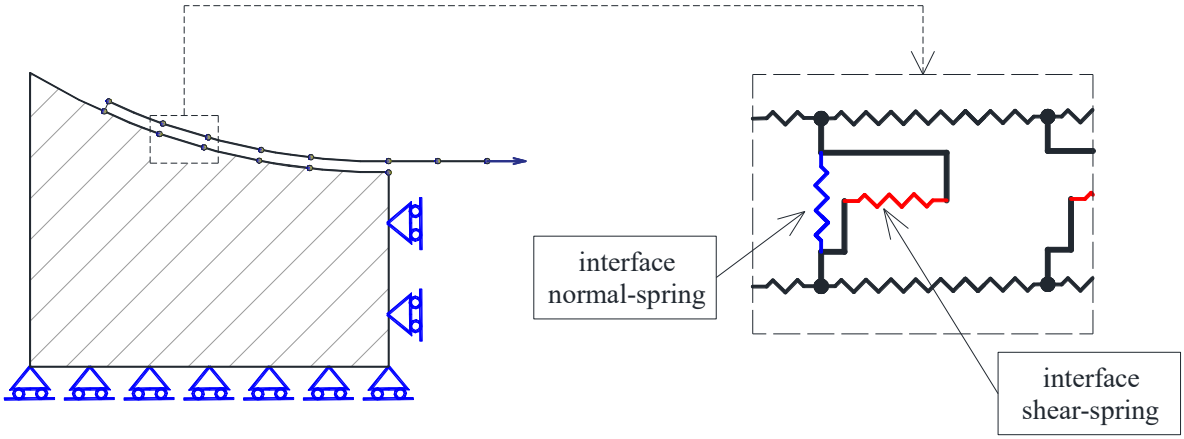

Figure 1. Schematization of the spring model.

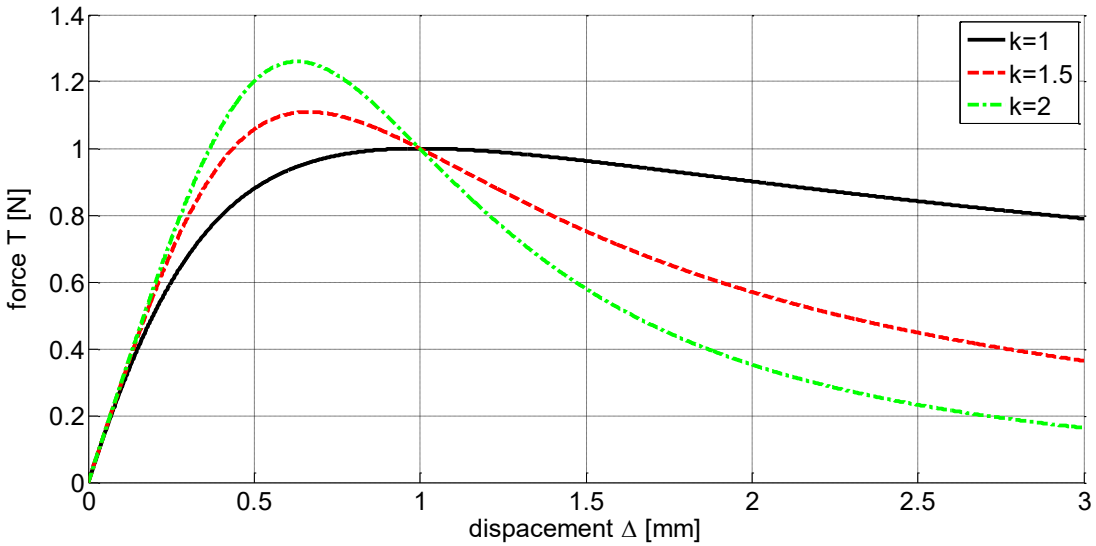

Figure 2. Influence of the coefficient k on the law proposed by Thorenfeldt et al. (1987). Accounted parameters: T_b=1 N; Δ_0=1mm; n=1.5.

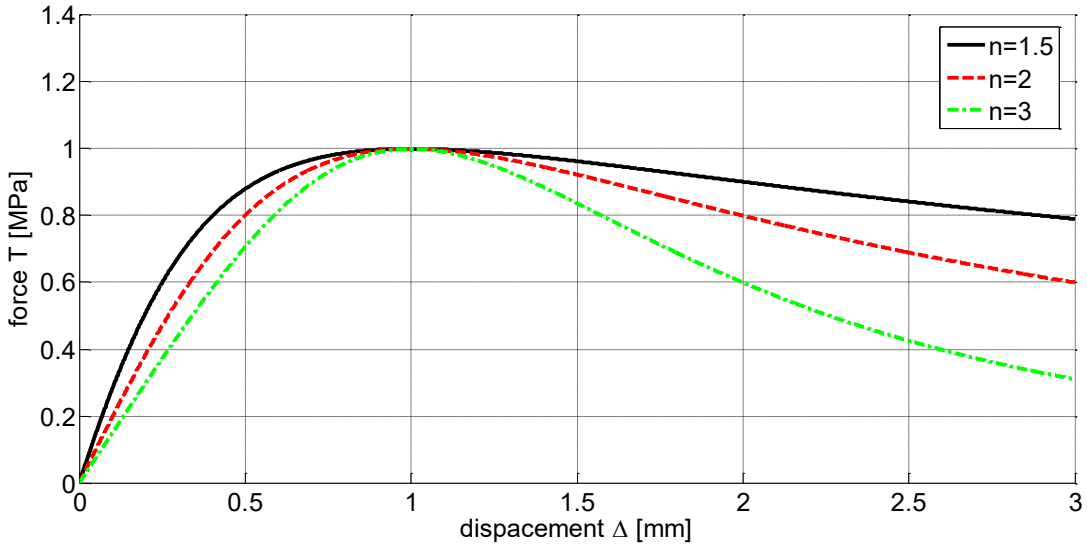

Figure 3. Influence of the coefficient n on the law proposed by Thorenfeldt et al. (1987). Accounted parameters: T_b=1 N; Δ_0=1mm; k=1.

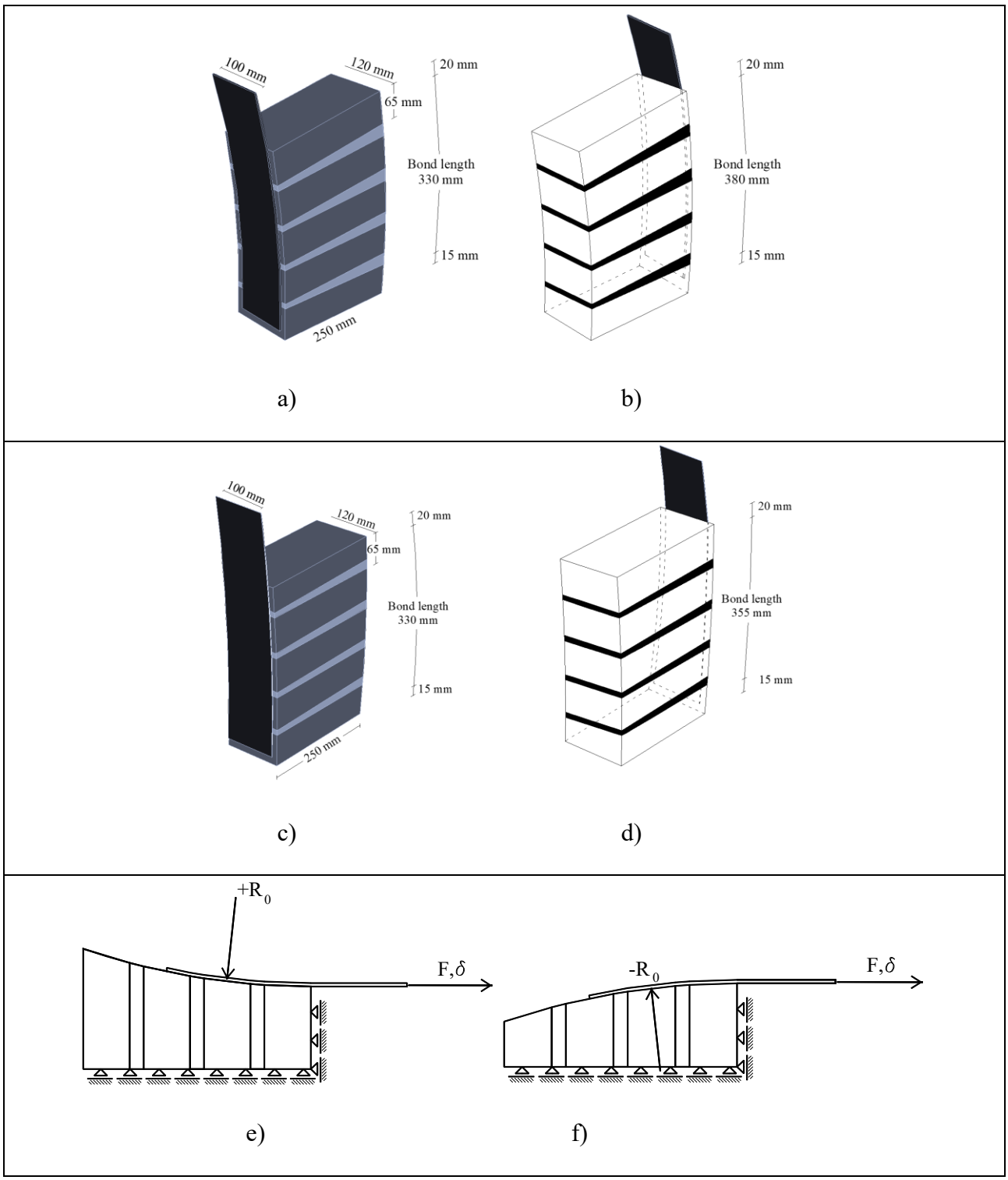

Figure 4. Specimen configurations used for numerical analyses: a) INTRADOS-R150 [Rotunno et al., 2018]; b) EXTRADOS-R150 [Rotunno et al., 2018]; c) INTRADOS-R300 [Rotunno et al., 2018]; d) EXTRADOS-R300 [Rotunno et al., 2018]; e) convex case [Basilio, 2007]; f) concave case [Basilio, 2007].

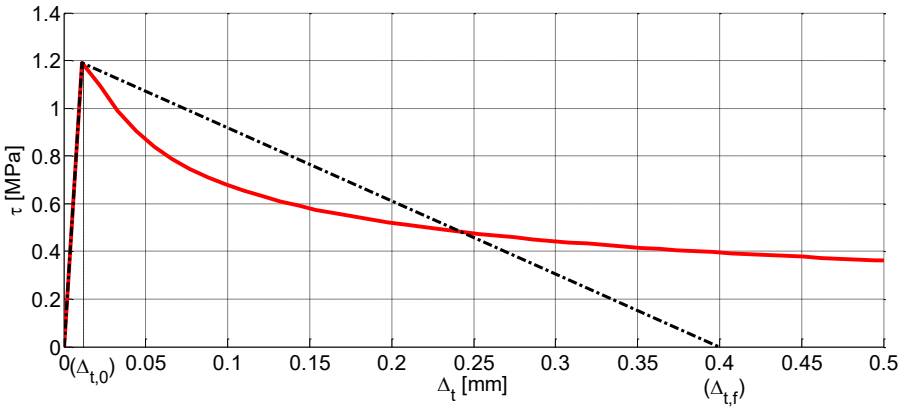

(a)

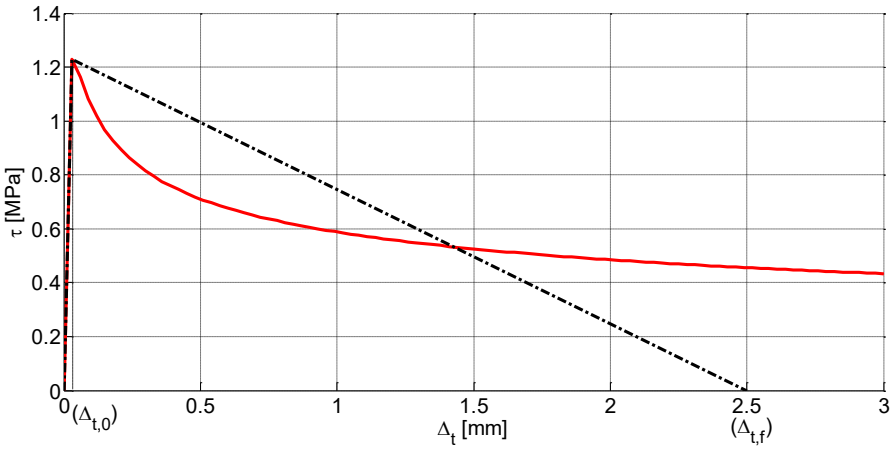

(b)

Figure 5. Bi-linear law (doted line) and Thorenfeldt's law (red line) accounted for the shear behavior of interfaces of (a) the specimens derived from Rotunno et al., 2018 and (b) the specimens derived from Basilio, 2007.

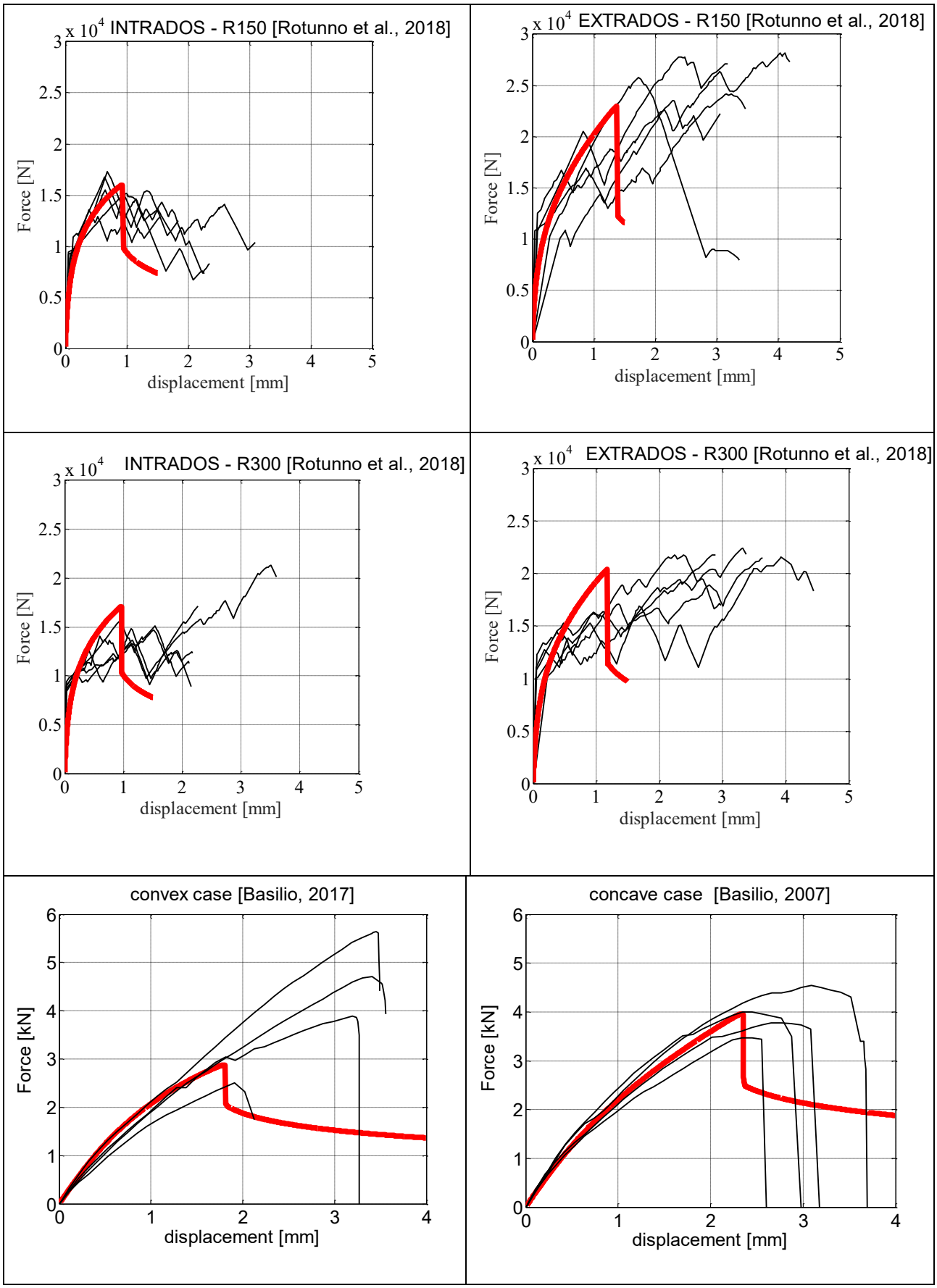

Figure 6. Results in terms of Force-displacement curves: comparison between experimental (thin black lines) and numerical results (thick red lines).

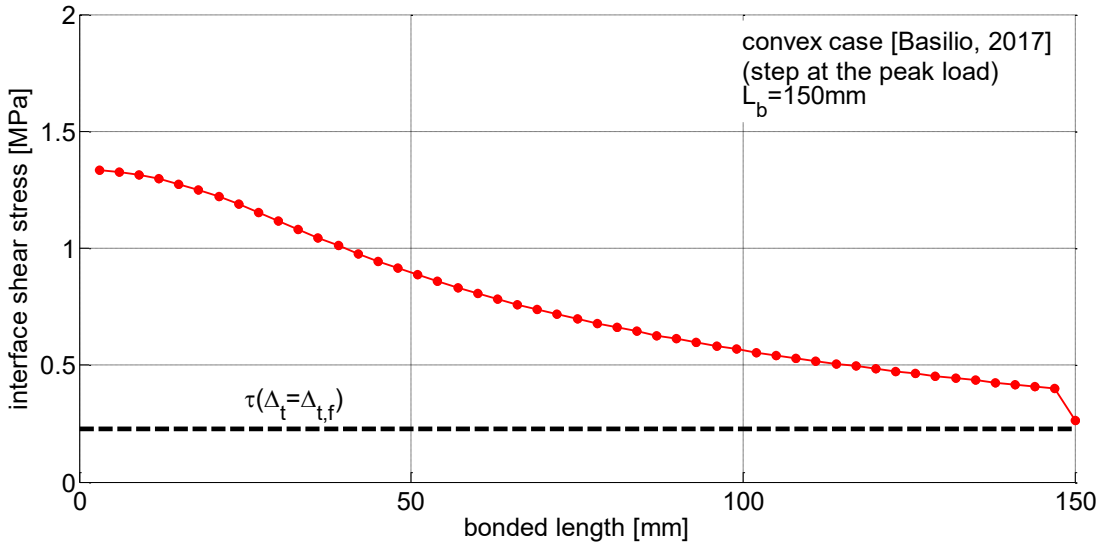

Figure 7. Shear stresses at the interface at the peak load (line with circular symbols) and shear stress level corresponding to the attainment of the ultimate displacement Δ_{tf} of shear springs (dotted line).